Atmosphere-Entry Behavior of a Modular, Disk-Shaped Isotope Heat Source

J. W. VORREITER,* J. J. BURNS,† W. C. PITTS,‡ AND H. A. STINE§
NASA Ames Research Center, Moffett Field, Calif.

The authors have studied the entry and impact behavior of an isotope heat source for space nuclear power that disassembles into a number of modules that would enter the Earth's atmosphere separately if a flight aborted. These modules are disk-shaped units, each with its own re-entry heat shield and protective impact container. In normal operation, the disk modules are stacked inside the generator, but during a re-entry abort they separate and fly as individual units of low ballistic coefficient. Flight tests at hypersonic speeds have confirmed that a stack of disks will separate and assume a flat-forward mode of flight. Free-fall tests of single disks have demonstrated a nominal impact velocity of 30 m/sec at sea level for a practical range of ballistic coefficients. Thermal and structural calculations indicate re-entry survival under all possible re-entry conditions for speeds up to and including Earth escape speed.

Introduction

THE protection requirements for space-destined nuclear materials have become more severe due to increasing environmental concerns, possible launch failure environments, and the demonstrated finite likelihood of booster malfunction.

Capsule damage resulting from ground impact after a re-entry abort is one motivation for developing a modular heat source. The problem of capsule impact damage can be solved in two ways. First, existing designs such as SNAP27 and SNAP19 can be improved by adding impact protection. Second (the solution used here), the kinetic energy at ground impact is reduced substantially by dividing the heat source into modular, disk-shaped units that, when released from the generator because of aerodynamic forces, fly as individual disks with a significantly lower mass-to-drag ratio than the assembled cylinder. This mass-to-drag ratio not only lowers the free-fall terminal velocity of individual disks as compared to other systems, but also reduces the aerodynamic heating environment during re-entry. In this paper, it is shown that such a heat source can be designed, adapted to existing generator systems, and thus will represent a viable solution to the problem of capsule damage.

The concept of a disk-shaped heat source is not new. The disk shape was briefly considered by Brunner et al.[1] but rejected because of uncertain aerodynamic performance. However, subsonic aerodynamic characteristics of flat objects including disks were investigated by Bustamante and Stone[2] among others and found to be systematic and predictable. Dix[3] discussed the disk as a possible solution to impact damage problems encountered on virtually all previous Radioisotope Thermoelectric Generator (RTG) programs. A tentative version of the design discussed here was considered by La Porte and Osmeyer.[4]

To consider the survivability of a disk module configuration, the authors first designed a modular disk-shaped heat source that would be compatible with existing RTG generators. Temperature distributions of the assembled heat source were first calculated for normal operation. These temperature levels were checked against known material compatibility results to appraise the desired long-life integrity and operation. Then this design was evaluated for re-entry survival if the launch vehicle malfunctioned. Several possible high-speed abort re-entry conditions were postulated for the modular heat source, and the thermal history of critical components was calculated for those conditions. The flat-forward mode of flight was experimentally confirmed by ballistic range tests at hypersonic speeds. The subsonic portion of flight after a high-speed abort re-entry was also experimentally investigated. Finally, the postimpact temperature of the modular heat source was calculated.

Presented at the 8th Intersociety Energy Conversion Engineering Conference, Philadelphia, Pa., August 13–17, 1973; submitted September 10, 1973; revision received December 19, 1973.

Index categories: Spacecraft Electric Power Systems; Entry Vehicle Mission Studies and Flight Mechanics.

* Research Scientist, Member AIAA.

† Staff Member, Los Alamos Scientific Laboratories.

‡ Research Scientist.

§ Assistant Division Chief, Thermo and Gas-Dynamic Division. Associate Fellow AIAA.

System Description

Figure 1 is an exploded view of an individual heat source module. The cost and fabrication of the fuel represent the major

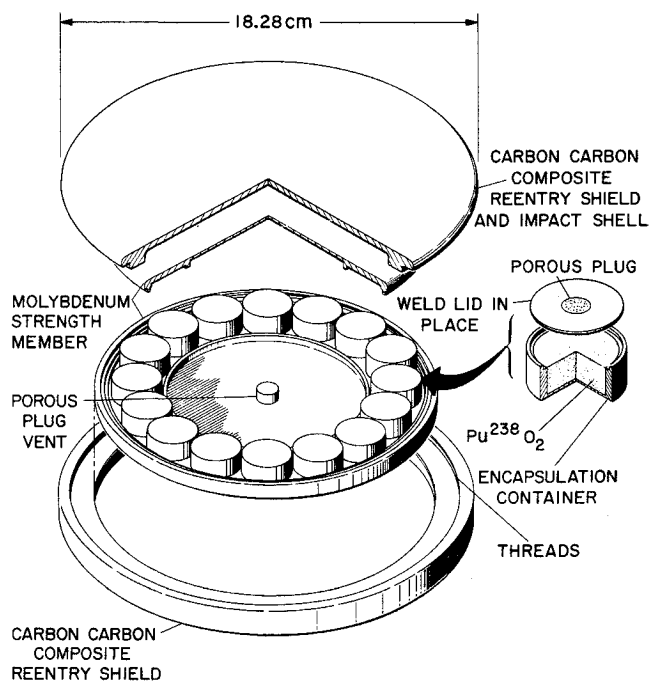

Fig. 1 Configuration of modular heat source.

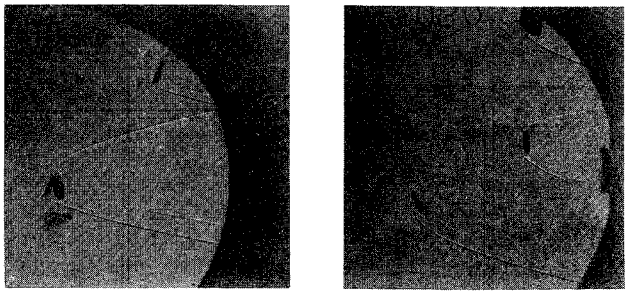

← Direction of flight

Fig. 2 Disk assembly in free flight—stabilization sequence.

Table 1 Comparison flight and test parameters at disk separation

Parameter	Range of flight parameters	Separation test	Stability test
Pressure (mm Hg)	0.04–3.3	1	100
Mach number	17–34	5.0	7.4
Reynolds number	11,000–400,000	2500	350,000
Thickness-diameter ratio	0.112	0.167	0.167
Ballistic coefficient (M/C_DA), kg/m^2	35.2	12.7	4.17
Dynamic pressure/ ballistic coefficient m/sec^2	180 → 4600	362	49,490

expense of most RTG systems. With that fact in mind, a fuel form in the shape of a right circular cylinder, 22.86 mm in diameter and 8.66 mm long, was chosen because it was easy to fabricate. The exact dimensions of the fuel pellet were chosen after dimension, thermal, and weight minimizations showed no optimum dimensions for the fuel form.

The fuel pellet is encapsulated in a container with a 0.254-mm thick wall made of some refractory noble metal alloy. Helium is vented from each fuel capsule through a porous plug. The container represents the primary barrier for long-term post-impact survival. In the arrangement studied, 16 encapsulated fuel pellets were deployed in an annular pattern and encased in a molybdenum alloy strength member. The wall of the strength member is 2.54-mm thick on the outer diameter, 1.25 mm on the top and bottom of the fuel annulus, and 0.254-mm thick on the top and bottom of the center cavity. The skin of the center cavity is supported in the center by a porous plug that vents helium to the environment. Molybdenum alloy was chosen as the primary strength member so that damage to the fuel pellets and their noble metal cans is minimized in the event of ground impact, blast, or fragment impact. The strength member also reduces the postimpact temperature. TZM was the particular alloy studied for this application because of its high strength/weight ratio and high melting temperature. TZM would, however, require a compatibility coating with high emissivity for this application.

The carbon-carbon composite re-entry heat shield surrounding the molybdenum strength member serves three functions: 1) as an ablative heat shield upon high-speed atmospheric re-entry; 2) as a barrier to high-speed fragments that might be generated in booster explosions; and 3) as a secondary strength member for ground impact. A carbon-carbon composite material was chosen for this shield because of its superior strength and high thermal shock resistance as compared with bulk graphites. The shield has a 182.9-mm o.d. and is 13.97-mm thick on the outer edge and 4.445-mm thick on the flat sides, with a 4.6-mm radius on the outside corner. The shield is two halves threaded together. To minimize stress concentrations caused by the threads, the shield was first structurally analyzed as a continuous body and then the threads were placed in an area of minimum stress. During normal operation, a number of modular disk heat sources are stacked to form the required system inventory.

Hypersonic Flight Tests

Before the aerodynamic advantages of the disk module design can be realized, two events must occur after the disk pack is separated from its container: the disks must separate from one another and each must assume a stable flat face-forward attitude. To determine whether both events will occur, the separation conditions were simulated in the Ames Hypervelocity Free-Flight Aerodynamic Facility. In this facility, models are fired from a light gas gun into a 36-m long chamber held at controlled pressure. Shadowgraph photographs are taken during flight. The pressure in the test chamber may be set at any value between several torr to several atmospheres.

A typical model consists of six brass or aluminum disks held together in a lexan sabot that is split axially into four segments. The sabot is designed to open by aerodynamic pressure as it leaves the gun muzzle. The model then flies down the range ahead of the sabot pieces.

A comparison is made in Table 1 between pertinent flight and test parameters. The flight values are for altitudes between 35 and 70 km. It was not practical to match the flight Mach number in this test, but the qualitative aerodynamic effects are expected to be the same for both flight and test Mach number ranges. The Reynolds number range was matched for flight altitudes above about 60 km. The thickness-to-diameter ratio for the test disks was 0.167 and the ballistic coefficient (M/C_DA) could not be matched because of material limitations. The dimensionless ratio of dynamic pressure to the ballistic coefficient, $q/(M/C_DA)$, was matched and varied to cover most of the expected flight range for this parameter. Since this parameter determines the deceleration of a body in unpowered flight, the time for separation and stabilization in the test should be comparable to that in actual flight.

Photographs were taken of the models during flight. They were launched with the disk pack axis aligned either normal or parallel to the direction of flight. A careful study of these photographs show that the disks quickly separate and fly as if they had been released as single bodies for all combinations of Reynolds and $q/M/C_DA$ investigated. For the separation tests $Re = 2500$ and $q/M/C_DA = 362$ m/sec^2.

The sequences of photographs in Fig. 2 show that the disks seek a stable flat face-forward attitude at hypersonic speeds. To observe the terminal phase of the disk flight, the deceleration was increased by increasing the dynamic pressure and by making the disks of aluminum to decrease the weight, hence (M/C_DA). For this phase, $q/(M/C_DA)$ was 49,490 m/sec^2. The leading disk and the other disks, while still in view, are shown rocking about the stable flat face-forward attitude.

None of the disks launched demonstrated an edge on stable flight attitude. This mode of flight is thought to be possible only at very high spin rates which are not likely to exist in an abort re-entry condition.

Free-Flight, Terminal Velocity Tests

Free-fall tests were conducted by Vorreiter and Tate[5] to determine the terminal velocity, to measure the lift-drag ratio and to measure differences in flight between identical bodies with different initial release conditions. The models were constructed of plexiglass and ballasted to match the shape, size, mass, and mass moment of inertia in both the axial and radial direction of the heat source module under study.

The disk modules were released by hand from the rear door of a C-130 aircraft flying at 4600 m altitude and were tracked to a low altitude by radar. The models were launched either with low spin rates and random attitude, horizontally spin-stabilized (flat down), or vertically spin-stabilized (edge down). No photographic coverage was available. The prevailing wind was measured vs

Table 2 Results of free-fall terminal velocity tests

Measurements	Models					
	A1	A2	A3	A4	A5	A6
Mass, kg	1.640	1.636	1.645	1.645	1.636	1.636
Initial conditions	Random low spin	Random low spin	Horizontally spin-stabilized	Horizontally spin-stabilized	Vertically spin-stabilized	Vertically spin-stabilized
Equivalent sea-level velocity, m/sec	29.134	28.892	31.360	30.189	26.70	28.35
Mean lift coefficient	0.305	0.309	0.176	0.263	0.408	0.321
Mean drag coefficient	1.135	1.153	1.002	1.065	1.332	1.196
C_L/C_D	0.268	0.264	0.175	0.246	0.306	0.268

altitude on the day of the test and subtracted from the observed motion to yield a "wind corrected" velocity vs altitude.

The x, y, and z velocity components deduced from the tracking radar for one of the drops are shown in Fig. 3 along with the total velocity V_T. The sinusoidal variation in the x and y velocity components indicates a spiraling motion. All but one of the randomly launched models flew in this helical pattern. None of the models launched either horizontally or vertically spin-stabilized edge down exhibited this behavior. This helical flight is explained by Vorreiter and Tate[5] as being due to a gyroscopic precession of a rotating body that has a displaced c.g. The data were also reduced to yield the mean lift and drag coefficients for each model in addition to a calculated terminal velocity at sea level (Table 2).

Noticeable differences existed between models launched with different initial attitudes. The models launched vertically spin-stabilized (edge down) demonstrated the lowest terminal velocity. The horizontally spin-stabilized models had the highest terminal velocity. The randomly launched were between these two extremes. The reasons for these differences are not known.

Re-Entry Analysis

Based on a study by Hogfors,[6] potential abort trajectories were calculated using the Ames Laboratory Trajectory Program (ALTRAJ), which is a finite-difference point mass program that uses a 1962 standard atmosphere and an oblate rotating Earth. Drag coefficients of 2.0, 1.8, and 1.18 were used for the free molecule, hypersonic continuum, and subsonic flow regions, respectively. A lift coefficient of 0.344 was used for the subsonic flow regime and since no autorotation was observed in any of our hypersonic free-flight tests, a zero lift coefficient was used in the calculation for supersonic speeds.

The trajectories were calculated in two different ways. First, for the majority of the calculations, the modular disk heat source was assumed to be a single re-entry body independent of the spacecraft and generator at an initial altitude of 122 km. Finally, to investigate the effects of spacecraft breakup on heat source survivability, the case of near-vertical entry at 10,180 m/sec was calculated using the ballistic coefficient of an intact generator as the initial condition. In this calculation, the ballistic coefficient was instantly changed to that of the modular disk heat source at various assumed breakup altitudes. This sudden exposure resulted in both an increase in deceleration and a sudden onset of aerodynamic heating.

The trajectory calculations also yielded a ground dispersal pattern for the heat sources which was circular, with a radius of about 10.2 km. The feasibility of recovery is not the subject of this study, but the search of such an area for lost nuclear payloads as described by Bustamante et al.[7] is fairly routine and has been conducted in the past.

Although over 20 detailed trajectories were calculated, only three will be discussed in detail. The entry at 10,180 m/sec and $-88°$ is of interest because it is the trajectory that causes the greatest thermal stresses in the heat shield and has the largest decelerations. The entry at 10,880 m/sec and $-25°$ yielded the highest internal temperatures of all those calculated. A large number of entries at speeds of 11,200 m/sec and various angles from $-5°$ to $-10°$ were investigated and all yielded much lower internal temperatures than the $-25°$, 10,880-m/sec trajectory. Therefore, the $-8°$, 11,201-m/sec trajectory was selected as typical of these shallow-angle trajectories.

The entry conditions that result in more than one pass through the atmosphere were analyzed on a parametric basis and are

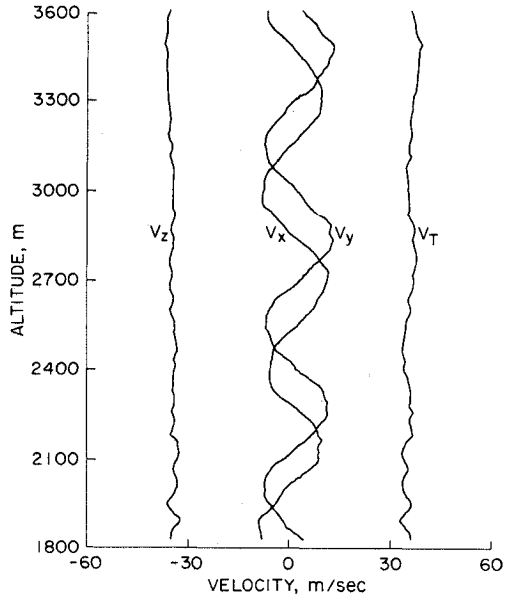

Fig. 3 Velocity vs altitude for free-falling disk module.

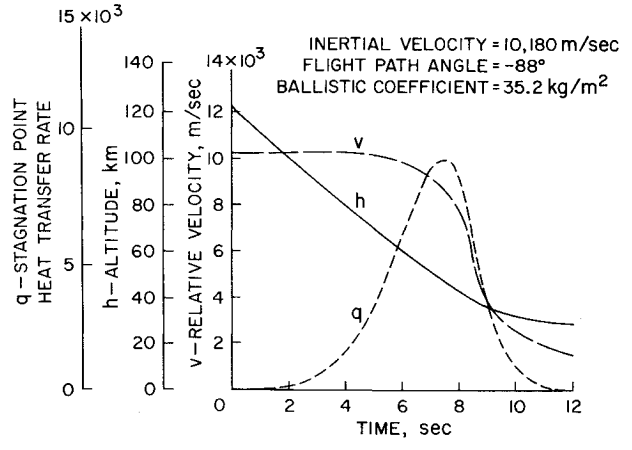

Fig. 4 Relative velocity, altitude, and stagnation heat-transfer rate vs time.

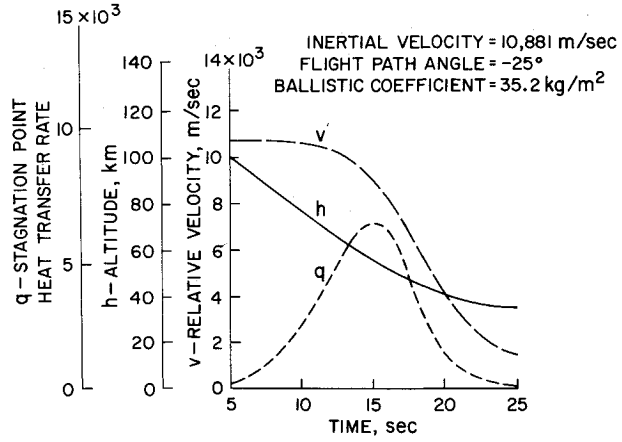

Fig. 5 Relative velocity, altitude, and reference heat-transfer rate vs time.

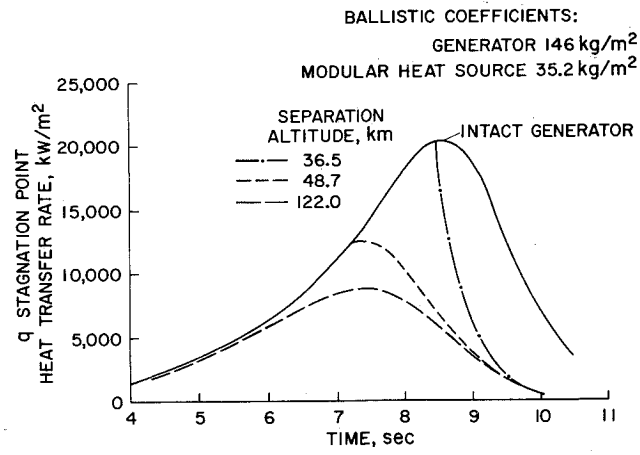

Fig. 7 Reference heating vs separation altitude (trajectory: 10,180 m/sec, $\gamma = -88°$).

discussed under "Ablation Analysis." The change in altitude, velocity, and stagnation point heat-transfer rate are shown as functions of time for these three trajectories in Figs. 4–6.

To investigate the effects of spacecraft breakup on the performance of the heat shield, the trajectory with entry conditions of $-88°$ and 10,180 m/sec was calculated with the generator breakup altitude treated as a parameter. The change in stagnation point heat-transfer rate for three different breakup altitudes is shown in Fig. 7.

Thermal Response

The distribution of heat-transfer rate around the end of a blunt cylinder as measured by Marvin and Sinclair[8] was used for the disk. Since the heat source is radially symmetric, except for the region around the fuel pellet, only the small portion of the unit shown in Fig. 8 needs to be thermally analyzed. The geometry was modeled with the Chrysler Improved Numerical Differencing Analyser (CINDA) transient heat-transfer program. The model contained 136 thermal elements or nodes. Considerable attention was given to the effects of the various gaps and voids shown in Fig. 8. When the external air pressure exceeded 0.005 atm, the gaps were assumed to be filled with air at a pressure of 1.0 atm. At external pressures lower than 0.005 atm, the gaps were assumed to be evacuated. The gap dimensions were adjusted continuously, depending on component thermal expansion coefficients and component temperatures. When deceleration exceeded 0.005 g, the gaps on the forward side were reduced to zero and the gaps on the rearward surface were doubled. The cold-wall heat input calculated in the trajectory analysis was continuously adjusted, depending on the enthalpy difference between the hot graphite surface and the surrounding gas cap. Corrections for ablative blowing were estimated and found to be very small for a body with this ballistic coefficient; thus they were not used. The normal operating temperature of the heat source within a helium-filled MHW generator are also shown in Fig. 8.

Figures 9–11 show the maximum temperatures in the shield, fuel, and strength member as a function of time for the three trajectories studied. At no time does any particular component exceed its melting temperature. Another unusual feature of this design (observable on these three figures) is that the external shield cools down very rapidly. This cooling is so rapid that, for all cases except the entry at $-88°$ and 10,180 m/sec, the temperature of the graphite shield dropped below the graphite oxidation limit of about 1350°K before the heat source fell to sufficiently low altitudes to encounter significant quantities of oxygen.

The mechanism of convective cooling during subsonic free fall after a high-speed re-entry was calculated by a Reynolds number correlation suggested by Kreith[9] for irregular objects. These approximate calculations indicate a shield temperature and a strength member temperature at ground impact of about 30° and 60°K above the ambient air temperatures, respectively.

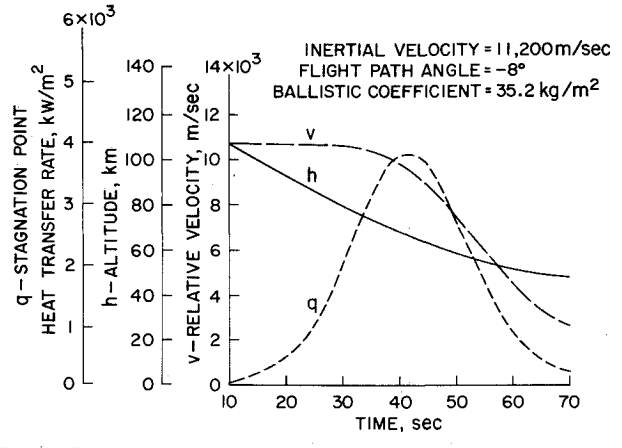

Fig. 6 Relative velocity, altitude, and reference heat-transfer rate vs time.

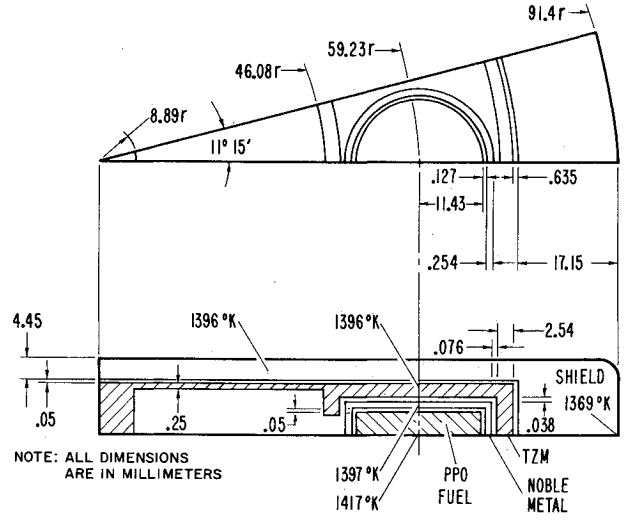

Fig. 8 Thermal model—240-W disk module at normal operating temperatures.

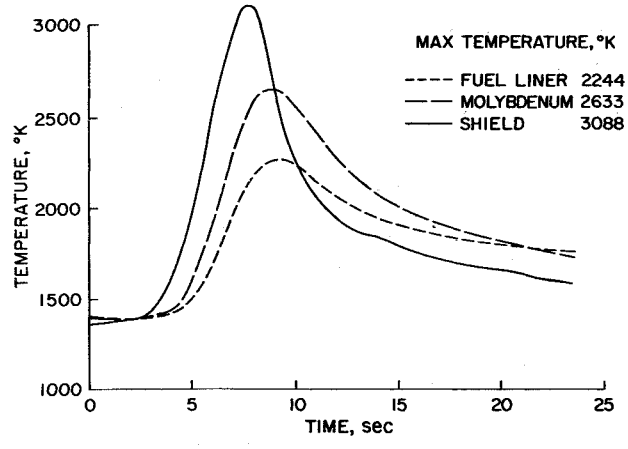

Fig. 9 240-W disk module; max component temperatures vs time, (−88°, 10,180-m/sec trajectory).

The temperature levels expected after ground impact were analyzed. The modular heat source was assumed to be stripped of its graphite heat shield and lying on coastal plain soil. The calculations assumed that the TZM strength member had a surface emissivity of 0.5 and was lying in still air. The results yielded a postimpact temperature of about 670°K which, although compatible with the noble metal fuel liner, will cause the TZM strength member to oxidize.

Structural Analysis

A stress analysis of the heat shield was made with the NASTRAN (NASA Structural Analysis) finite-element computer program. Thermal, pressure, and inertia loads were included. The inertia loads due to aerodynamic deceleration of the fuel and strength members were distributed uniformly over the inner portion of the shield. The body-inertia force of the heat shield was accounted for in the NASTRAN program as were the thermal load forces. The pressure load was obtained from the calculated stagnation pressure and the pressure distribution profile given in Inouye et al.[10] The finite-element model used in the analysis is shown in Fig. 12 along with the manner in which the loads were applied.

Input data for the stress analysis were obtained from the thermal and re-entry analyses previously described. Stress in the heat shield was calculated for the five release altitudes: 36.5, 48.7, 57.9, 76.1, and 122 km. For each case, stresses were calculated for thermal loads only and for combined thermal, pressure, and inertia loads. The material properties[11] used in these calculations are shown in Table 3.

Lines of constant stress are plotted in Figs. 13 and 14 for conditions when the release altitude is 36.5 km, the most severe

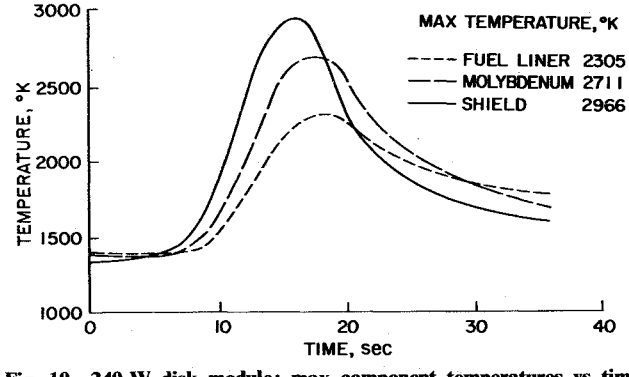

Fig. 10 240-W disk module; max component temperatures vs time (−25°, 10,881-m/sec trajectory).

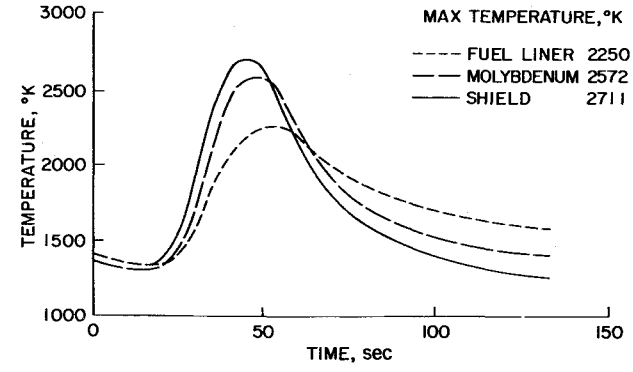

Fig. 11 240-W disk module; max component temperatures vs time (−8°, 11,186-m/sec trajectory).

case examined. The lines of constant stress continue from the left to the center of the heat shield as essentially parallel lines. The corresponding plots for other release altitudes are qualitatively the same as those shown for the 36.5-km release altitude. It is generally true that, for all conditions, circumferential stress is larger than radial stress and axial stress is negligibly small. Adding pressure and inertia loads increases the magnitude of the maximum stress, particularly the circumferential stress. For the heat shield, these stresses are well within the ultimate stress limits of 90×10^6 to 120×10^6 N/m^2 in tension and 90×10^6 to 165×10^6 N/m^2 in compression (depending on temperature). A summary of the maximum (circumferential) stresses for the heat shield is shown in Fig. 15 as a function of the release altitude.

Table 3 Thermophysical properties of carbon-carbon composite heat shield[11]

Property	293°K	1273°K	2200°K
Elastic modulus, 10^9 N/m^2	29		20
Thermal coefficient of expansion, 10^{-6} m/m/°K	−0.9	1.8	3.4
Poisson's ratio	0.15		0.15
Ultimate tensile strength, 10^6 N/m^2	90		120
Ultimate compressive strength, 10^6 N/m^2	90		165

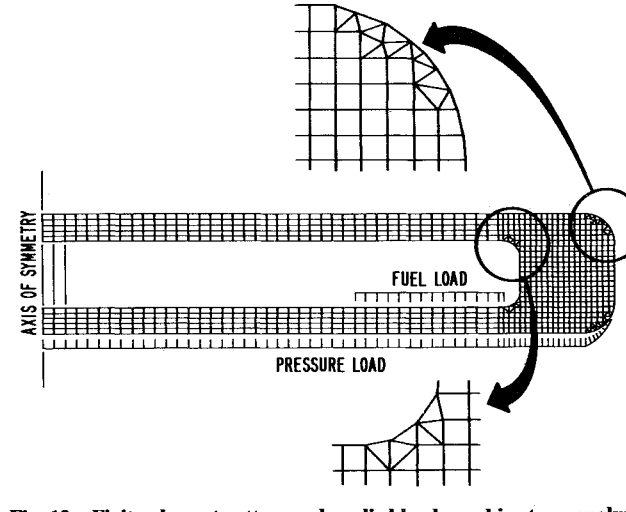

Fig. 12 Finite-element pattern and applied loads used in stress analysis of heat shield.

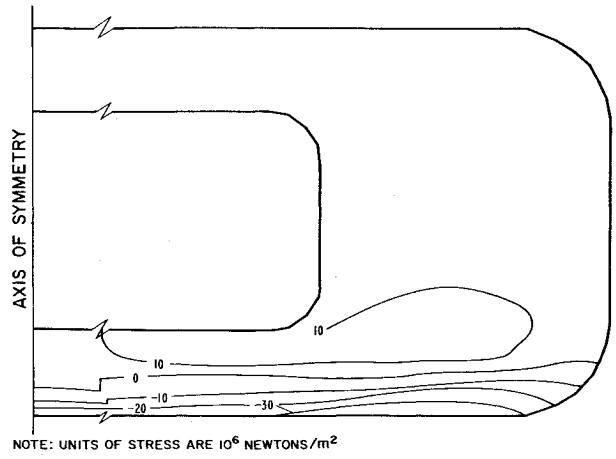

Fig. 13 Lines of constant radial stress in heat shield for thermal, pressure, and inertia loads; entry angle = −88°, velocity = 10,180 m/sec, release altitude = 36.5 km.

Ablation Analysis

The ablation of the graphite heat shield was investigated for many trajectories including both single and multipass entries. The calculations used the ablation equations of Metzger et al.[12] in the reaction limited regime, of Scala and Gilbert[13] in the diffusion limited regime, and of Scala and Gilbert[14] in the sublimation regime. The ablation was found to be significant only in two cases. For the entry at −88° and 10,180 m/sec, the ablation during the subsonic and hypersonic portions of the flight was 0.85 and 0.25 mm, respectively, for a total of 1.1 mm.

The range of entry angles that results in multiple passes through the Earth's atmosphere was investigated and the ablation vs entry angle is shown in Fig. 16. For the worst multipass entry condition, only 2.5 mm of graphite would be ablated from the original 4.45 mm of material.

Conclusions

The design of a disk-shaped isotope heat source under atmospheric entry conditions has been evaluated. If stacks of disks are launched at hypersonic speeds, the disks quickly separate and fly as individual units in a flat-forward attitude. When released from an aircraft at high altitude, the disks were observed by radar to fly in a predominant spiral autorotating flight pattern with an equivalent terminal velocity of 29.1 m/sec at sea level. Considerable effort was expended to predict the thermal and structural responses of the modular disk heat source to a variety of potential Earth entry environments. It was found that no component of the heat source overheated during re-entry and the stresses induced by temperature gradients, pressures, and dynamic loads were far below the expected failure stresses of the heat-shield material. The amount of ablation that would occur for a variety of re-entry situations was calculated and found to be well below the selected ablator thickness.

It is believed that the modular disk heat source is a practical solution to the more severe abort re-entry environments that can be expected on future space missions, and that the low terminal

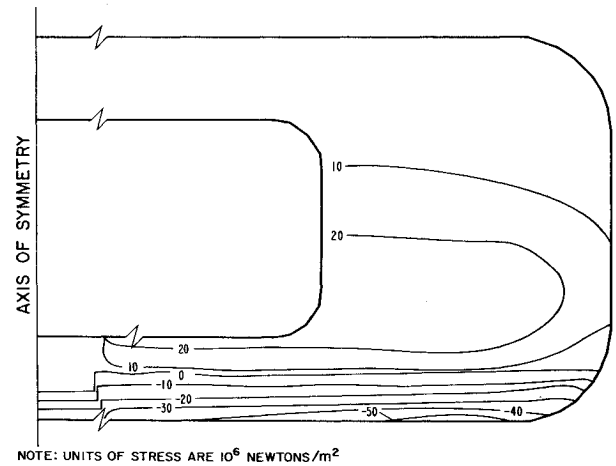

Fig. 14 Lines of constant circumferential stress in heat shield for thermal, pressure, and inertia loads; entry angle = −88°, velocity = 10,180 m/sec, release altitude = 36.5 km.

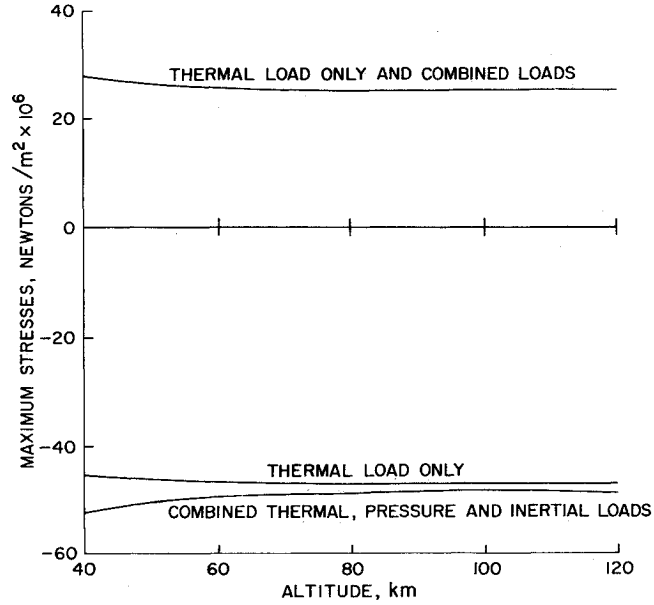

Fig. 15 Dependence of heat-shield maximum circumferential stress on release altitude.

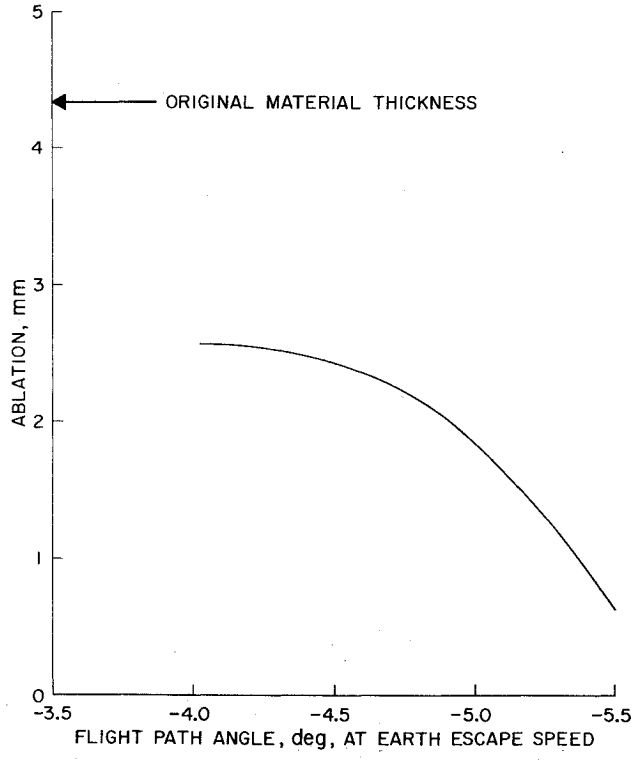

Fig. 16 Ablation of modular heat source (multipass re-entries).

velocity at sea level of these units represents a viable solution to the problem of ground impact damage that has plagued almost all space nuclear heat source programs to date.

References

[1] Brunner, M. J., Dohner, C. V., and Lawit, R. L., "Re-Entry of Radioactive Power Sources," *Journal of Spacecraft and Rockets*, Vol. 5, No. 4, April 1968, pp. 448–453.

[2] Bustamante, A. C. and Stone, G. W., Jr., "The Dynamic Characteristics of Autorotating Configurations in Subsonic and Hypersonic Flows," SC-DE-682395, Nov. 1968, Sandia Labs., Albuquerque, N.Mex.

[3] Dix, G. P., "Advances in the Safety of Space Nuclear Power Systems," Second International Symposium on Power from Radioisotopes, European Nuclear Energy Agency and Spanish Junta on Atomic Energy, Madrid, Spain, May 1972.

[4] La Porte, A. H. and Osmeyer, W. E., "Growth Potential of the Snap 19 High Performance Generator Through Technology Application," International Conference on Nuclear Solutions to World Energy Problems, American Nuclear Society, Washington, D.C., Nov. 1972.

[5] Vorreiter, J. W. and Tate, D. L., "Observations of Disk-Shaped Bodies in Free Flight at Terminal Velocity," TM X-62, 262, 1973, NASA.

[6] Hogfors, H. E., "Velocity-Flight Path Envelopes for Different Failure Modes in a Titan IIIC Synchronous Mission," TOR-0172-(2701-01)-5, March 6, 1973, Aerospace Corp., El Segundo, Calif.

[7] Bustamante, A. C., Randall, D. E., and McAlees, S., "Have Sinew-1 Postflight Report," SC-RR-72 0225, May 1972, Sandia Labs., Albuquerque, N.Mex.

[8] Marvin, J. G. and Sinclair, A. R., "Convective Heating in Regions of Large Favorable Pressure Gradient," *AIAA Journal*, Vol. 5, No. 11, Nov. 1967, pp. 1940–1948.

[9] Kreith, F., *Principles of Heat Transfer*, International Textbook Co., Scranton, Pa., 1958, p. 379.

[10] Inouye, M., Marvin, J. G., and Sinclair, A. R., "Comparison of Experimental and Theoretical Shock Shapes and Pressures Distributions on Flat-Faced Cylinders at Mach 10.5," TN D-4397, 1968, NASA.

[11] "Mechanical and Thermal Properties of MOD-3 Billets 727 and 731," Purchase Order 236041, Prime Contract F33615-70-C-1587, April 28, 1972, Southern Research Inst., Birmingham, Ala.

[12] Metzger, J. W., Engel, M. J., and Diaconis, N. S., "The Oxidation and Sublimation of Graphite in Simulated Re-Entry Environments," AIAA Paper 65-643, Monterey, Calif., 1965.

[13] Scala, S. M. and Gilbert, L. M., "Aerothermochemical Behavior of Graphite at Elevated Temperatures," Rept. R63SD89, Nov. 1963, General Electric, King of Prussia, Pa.

[14] Scala, S. M. and Gilbert, L. M., "Sublimation of Graphite at Hypersonic Speeds," *AIAA Journal*, Vol. 3, No. 9, Sept. 1965, pp. 1635–1644.

MAY 1974 J. SPACECRAFT VOL. 11, NO. 5

Four Space Shuttle Wing Leading Edge Concepts

G. A. NIBLOCK* AND J. C. REEDER†
McDonnell Douglas Astronautics Company-East, St. Louis, Mo.

AND

F. HUNEIDI‡
Marshall Space Flight Center, Huntsville, Ala.

A heat-pipe-cooled Space Shuttle orbiter wing leading edge was compared and evaluated against three alternate leading edge candidates: a refurbishable ablative design, and two other reusable versions employing coated columbium and carbon-carbon high-temperature segments. Each candidate concept was shown feasible in the Phase B environment. The reusable versions were all found to cost nearly the same and substantially less than the nonreusable ablative version.

Nomenclature

Aw = cross sectional area of wick
g = acceleration
g_c = gravitational constant
h_{fg} = heat of vaporization
K_p = permeability constant
$K_p A_w/W$ = wick design parameter
q_o = stagnation heat flux
$q(x)$ = local heat flux
$q(x)/q_o$ = ratio of local to stagnation heat flux
r_c = capillary radius
W = wick thickness
x = distance along heat pipe axis
Z = axial length
ΔP_c = available capillary pumping pressure rise
ΔP_g = pressure due to gravity
ΔP_L = liquid pressure drop
ΔP_v = vapor pressure drop
θ = contact angle
μ_L = liquid viscosity
μ_v = vapor viscosity
ρ_L = liquid density
σ = surface tension
ϕ = angle between axis of heat pipe and acceleration vector

Presented as Paper 73-738 at the AIAA 8th Thermophysics Conference, Palm Springs, Calif., July 16–18, 1973; submitted August 15, 1973; revision received November 30, 1973.

Index categories: Spacecraft Temperature Control Systems; Structural Design, Optimal.

* Senior Thermodynamics Engineer.

† Senior Strength Engineer.

‡ Technical Assistant to Thermal Engineering Branch Chief, Astronautics Laboratory.

I. Introduction

THE goal of low-cost space transportation that the Space Shuttle is expected to accomplish requires reusable system components. The orbiter will make about 100 flights in fulfilling its design capability. During the flights the nose region and leading edge surfaces experience an extremely severe environment.

A study was performed under Contract NAS 8-27708 to examine the feasibility of using high-temperature heat pipes for cooling nose and wing stagnation regions and three alternate concepts for the wing application. The orbiter leading edge heat